LA-UR-85-2994

DE85 017539

CONF-8506109--2

Los Alamos National Laboratory is operated by the University of California for the United States Department of Energy under contract W-7405-ENG-36

TITLE: REACTIVE SCATTERING IN THE BENDING-CORRECTED ROTATING LINEAR MODEL

AUTHOR(S): R. B. Walker
E. F. Hayes

SUBMITTED TO: Proceedings of CECAM/NATO Workshop on Chemical Reaction Dynamics
NATO ASI Series
Orsay, France, June 17-28, 1985

DISCLAIMER

Los Alamos Los Alamos National Laboratory
Los Alamos, New Mexico 87545

FORM NO 836 R4
ST NO 2629 5/81

final version

REACTIVE SCATTERING IN THE BENDING-CORRECTED ROTATING LINEAR MODEL

Robert B. Walker
Group T-12, MS J569
Theoretical Division
Los Alamos National Laboratory
Los Alamos, NM 87545

Edward F. Hayes
Controllers Office
National Science Foundation
Washington, DC 20550

ABSTRACT. We review the theory and applications of the Bending-Corrected Rotating Linear Model (BCRLM) to problems in the quantum description of reactions between atoms and diatomic molecules.

1. INTRODUCTION TO BCRLM

The Bending-Corrected Rotating Linear Model (BCRLM) is a straightforward extension of the Rotating Linear Model (RLM) proposed in the late 1960's by Child,[1] Wyatt,[2] and Connor and Child.[3] The RLM constrains the dynamics of three dimensional (3D) collisions by requiring the molecular species to maintain an orientation collinear with the atomic species during the course of collision. The classical dynamics of three particles on a line was considered prior to this by Jepsen and Hirschfelder,[4] and more recently by Agmon,[5] but the BCRLM is an outgrowth of the model presented by the authors of Refs. 1-3.

By neglecting the two internal rotational (or bending) degrees of freedom, the mathematical description of the rearrangement collision event is simplified so extensively that the computational treatment of reaction dynamics within this model is routinely possible. This computational simplication arises because the rotational motion of the line of collision is treated analytically by a partial wave expansion of the scattering wavefunction. Consequently, the computational effort reduces to that of a family of collinear reactive scattering calculations, one for each partial wave term in the wavefunction expansion.

The obvious shortcoming of the RLM is its neglect of the internal rotational degrees of freedom. In comparison to the asymptotic vibrational degrees of freedom, the asymptotic rotational degrees of freedom impose a relatively modest constraint on the energetics of collision.

but they correlate adiabatically to higher energy bending states when the collision partners are close together. The results of the earliest accurate 2D and 3D coupled-channel calculations[6-14] for the $H+H_2$ reaction showed that these bending degrees of freedom are important in determining the energetic position of the reaction threshold. Consequently, Walker and Hayes[15] implemented the suggestion made in Wyatt's[2] paper, and supplemented the RLM with an ad hoc correction to include the adiabatic effects of the lowest energy bending degrees of freedom, producing the bending-corrected RLM, or BCRLM. Including the bending degrees of freedom as an effective potential within a collinear reactive framework was first described by Mortensen and Pitzer[16,17] and is now widely used by Bowman and coworkers[18-24] in reduced dimensionality theories of reaction, and by Truhlar and coworkers[25-32] in variational transition state theories of reactions.

In practice, all BCRLM calculations to date have been done so that only the lowest energy (i.e., zero point) bending state has been explicitly treated. At this level, the additional computational effort for a BCRLM calculation instead of an RLM calculation is minimal -- it is necessary only to compute an effective collinear potential energy surface which is the sum of the usual collinear potential and the bending zero point energy determined at each collinear geometry. In principle, however, a full treatment of the bending degrees of freedom within the adiabatic approximation would require a family of RLM calculations, one for each bending state.

Another obvious defect of both the RLM and BCRLM models is that they assume a collinearly dominated reaction intermediate. While the potential energy surfaces for many collision systems do favor collinear geometries, there are of course many reactions which do not. Extensions of the BCRLM model are therefore needed to treat noncollinear systems, perhaps along the lines defined by the Carrington and Miller[33] reaction surface Hamiltonian theory.

In the next section (Sec. 2), we will develop the theory of the BCRLM. We discuss the solution of the coupled-channel equations in both natural collision coordinates[34-38] and hyperspherical coordinates.[39-47] Both coordinate systems are widely used to treat collinear reactive scattering processes. We will discuss the projection[48,49] of the hyperspherical equations on coordinate surfaces appropriate for applying scattering boundary conditions and review the definition of integral and differential scattering cross sections in this model.

In Sec. 3, we will briefly review applications of BCRLM calculations to reactive systems and discuss in Sec. 4 some possible future developments which may be made through extensions of the method. Sec. 5 then concludes with a summary.

2. THEORY

In this section, we will present a mathematical description of the BCRLM. We will define the classical and quantum mechanical Hamiltonian for the translational, vibrational, tumbling, and bending degrees of freedom for the system. After expanding the scattering wavefunction in

a total angular momentum representation, we obtain coupled-channel equations which may be solved numerically subject to reactive scattering boundary conditions. The solution of these coupled-channel equations at a fixed total scattering energy E and angular momentum J determines the scattering matrix, $\underline{S}^{J}(E)$. From the scattering matrix, we can then compute reaction probabilities, integral and differential cross sections, and reaction rate constants.

2.1. Internal Coordinate Systems

We restrict ourselves here to the atom-diatom reactive collision process defined chemically by the equation

$$A + BC(m) \rightarrow AB(n) + C, \tag{1}$$

in which A and BC are the reactant atom and molecule respectively, and AB and C are the product molecule and atom. The vibrational quantum numbers of the reactant and product molecules are m and n respectively. We further assume that the collision dynamics is represented by the motion of the A, B, and C nuclei on a single Born-Oppenheimer electronic potential energy surface, at energies below the threshold for collision induced dissociation. The atomic masses are defined as m_A, m_B, and m_C.

Coupled-channel equations arise in scattering dynamics when all but one of the degrees of freedom of the system are expanded in a square integral basis (of "channels"). The coupled-channel equations are then solved numerically and describe motion in the unbound, or scattering coordinate. The principal difficulty of any reactive scattering calculation is that the coordinate system which best describes the asymptotic motions of reactants differs from the coordinate system best suited for products. Consequently, computational methods commonly use different coordinate systems in different parts of configuration space. Boundary conditions are expressed in terms of Jacobi coordinates (sometimes referred to as "cartesian coordinates"), where in the A+BC arrangement r_{BC} is the internuclear separation of the BC molecule,

$$r_{BC} = |\vec{r}_{BC}| = |\vec{r}_B - \vec{r}_C|, \tag{2}$$

and $R_{A,BC}$ is the distance between the atom and the center of mass of the BC molecule,

$$R_{A,BC} = |\vec{R}_{A,BC}| = \left|\vec{r}_C - \frac{m_A\vec{r}_A + m_B\vec{r}_B}{m_A + m_B}\right|. \tag{3}$$

In Eqs. (2) and (3), the vectors $\vec{r}_A$, $\vec{r}_B$, and $\vec{r}_C$ locate the atoms A, B, and C, respectively, relative to an origin of a space-fixed Cartesian reference frame, and $|\vec{r}|$ denotes the length of the vector $\vec{r}$. Equations

analogous to (2) and (3) are obtained for the B + AC and C + AB arrangements by cyclically permuting the A, B, and C labels, and define the appropriate Jacobi coordinates for other asymptotic configurations. Because the RLM and BCRLM consider only collinear or near-collinear reaction intermediates, only a single arrangement of product species is possible (as in Eq. (1)), and so we need to consider only the Jacobi coordinates for A+BC geometries (the α arrangement) and AB+C geometries (the γ arrangement). We then define mass-scaled Jacobi coordinates so that motion in both r and R occurs with the same effective reduced mass. These coordinates are

$$
\begin{aligned}
R_\alpha &= C_\alpha^{-1} R_{A,BC} , \qquad R_\gamma = C_\gamma^{-1} R_{C,AB} , \\
r_\alpha &= C_\alpha r_{BC} , \qquad r_\gamma = C_\gamma r_{AB} , \\
C_\alpha^4 &= \left[\frac{(m_A + m_B + m_C) m_B m_C}{m_A (m_B + m_C)^2} \right] .
\end{aligned}
\tag{4}
$$

Early treatments of collinear reaction dynamics addressed the coordinate problems associated with different asymptotic arrangement channels by using natural collision coordinates.[34-38] The generic

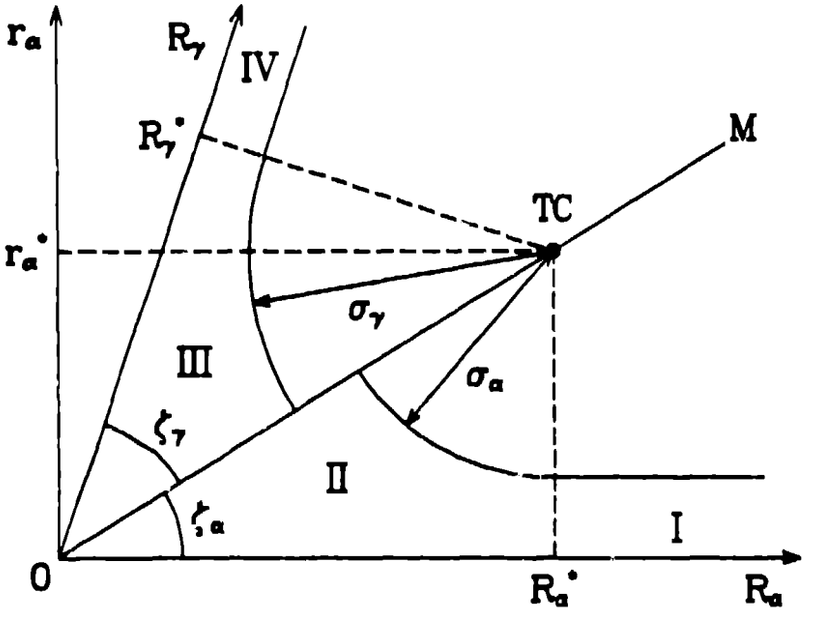

Figure 1. Collinear configuration space, subdivided into regions (I-IV) in which different coordinate systems are used. Regions I and II are for reactants, and III and IV are for products. M is a matching line between reactants and products, and TC is the origin of the polar natural collision coordinates used in Regions II and III.

feature these curvilinear coordinate systems share is that they deform smoothly from the Jacobi coordinates of reactants to the Jacobi coordinates of products. In practice, BCRLM calculations[18] have used natural collision coordinates[49] which can be visualized with the aid of Fig. 1. The NCC are actually plane polar coordinates with an origin located at a turning center labelled TC in Figure 1. The TC has projections R_α^* and r_α^* on the α axes and R_γ^* and r_γ^* on the γ axes. For computational purposes, the collinear configuration space (between the R_α and R_γ axes in Fig. 1) is divided into four regions. Regions I and II (reactants) are separated by a matching surface M from regions III and IV (products). In region I, containing geometries in which $R_\alpha > R_\alpha^*$, and $\tan^{-1}(r_\alpha/R_\alpha) < \gamma_\alpha$, Jacobi coordinates R_α and r_α are used. Similarly, in Region IV, Jacobi coordinates R_γ and r_γ are used. Natural collision coordinates u_α and v_α are used for configurations in Region II, within the triangle defined by (O, TC, R_α^*); coordinates u_γ and v_γ are used in Region III, within the triangle defined by (O, TC, R_γ^*). In terms of R_α and r_α, u_α and v_α are

$$\begin{aligned} R_\alpha &= R_\alpha^* - \eta_\alpha \sigma_\alpha \sin\tau_\alpha, \\ r_\alpha &= r_\alpha^* - \eta_\alpha \sigma_\alpha \cos\tau_\alpha, \\ \eta_\alpha &= 1 + v_\alpha/\sigma_\alpha, \\ \tau_\alpha &= \pi/2 - \zeta_\alpha - u_\alpha/\sigma_\alpha. \end{aligned} \tag{5}$$

Equations analogous to Eq. (5) define R_γ and r_γ in terms of u_γ and v_γ.

Natural collision coordinates defined in this way are convenient for many reactive systems but have the drawback that one must decide where to locate the turning center TC. Physical considerations require that it be placed far away from the origin, in a region of sufficiently high potential energy that the scattering wavefunction, once determined, will be negligibly small there. This requirement immediately implies that these coordinates are unsuitable at scattering energies above the threshold for collision induced dissociation.

A second problem is encountered for "heavy-light-heavy" (HLH) systems in which the mass of the transferred atom B is small in comparison to the masses of A and C. In such cases, the skew angle ($\zeta_{\alpha\gamma} = \zeta_\alpha + \zeta_\gamma$, see Fig. 1) becomes very small, and tunneling between the reactant and product valleys may occur at large distances, requiring that TC be located far from the origin. When this is done, the vibrational motion of the system is poorly represented by the v coordinate. Consequently, slices of the potential at fixed values of u generate

broad effective vibrational wells whose shape changes rapidly with u. As a result, a large basis of target functions in the v coordinate is required in the coupled-channel equations at each of a large number of integration steps in the coordinate u.

It is more economical to use hyperspherical coordinate systems[39-47] for HLH systems. For collinear configurations, these coordinates are also plane polar coordinates, but the turning center is located at the origin. These coordinates have had a wide application to collinear reactions,[50-61] especially those of the HLH variety. The hyperspherical radius ρ is independent of the arrangement channel index

$$\rho^2 = R_\alpha^2 + r_\alpha^2 = R_\gamma^2 + r_\gamma^2, \qquad 0 \le \rho < \infty, \tag{6}$$

and the hyperspherical angle depends in a simple way on α or γ

$$\begin{aligned} &\tan\varphi = r_\alpha/R_\alpha, \\ &\tan(\varsigma_{\alpha\gamma}-\varphi) = r_\gamma/R_\gamma, \qquad 0 \le \varphi \le \varsigma_{\alpha\gamma}. \end{aligned} \tag{7}$$

Whether the numerical problem is solved in natural collision coordinates or in hyperspherical coordinates, we still must express boundary conditions in the appropriate asymptotic Jacobi coordinates. In the natural collision coordinates of Fig. 1, there is a common boundary between Regions I and II in the α coordinates, between Regions III and IV in γ coordinates, and between Regions II and III separating arrangement channels. In a hyperspherical approach, however, the boundaries between regions which employ different coordinates do not match, as in Fig. 2. Consequently, we must numerically project the solutions of Schrodinger's equation inside the hyperspherical region onto constant R_α and R_γ surfaces. This projection is more complicated in comparison to the analagous but analytic projection procedures[49] required in the NCC approach. This asymptotic matching requirement may be regarded as a minor disadvantage of hyperspherical coordinates.

2.2. The Classical Kinetic Energy

The classical kinetic energy of an A+BC system in a 3D center-of-mass frame may be written in mass-scaled α Jacobi coordinates as

$$T_\alpha = \mu/2\left[\dot{R}_\alpha^2 + \dot{r}_\alpha^2 + R_\alpha^2(\dot{\theta}_\alpha^2+\sin^2\theta_\alpha\dot{\phi}_\alpha^2) + r_\alpha^2(\dot{\xi}_\alpha^2+\sin^2\xi_\alpha\dot{\nu}_\alpha^2)\right], \tag{8}$$

where μ is a reduced mass common to all arrangements (because of the mass scaling of Eq. (4)),

$$\mu = \left[\frac{m_A m_B m_C}{(m_A+m_B+m_C)^2}\right]^{1/2}. \tag{9}$$

In Eq. (9), θ_α and ϕ_α are the spherical polar angles of the $\vec{R}_\alpha$ vector in a space-fixed coordinate frame (see Eqs. (3) and (4)), and ℓ_α and ν_α are the corresponding spherical polar angles of the $\vec{r}_\alpha$ vector.

The essence of the approximation in the RLM is to require that both $\vec{r}_\alpha$ and $\vec{R}_\alpha$ be parallel, and hence their spherical polar angles are equal. The atoms A, B, and C now lie on a line in 3D, whose spherical polar angles are defined as θ and ϕ, so that

$$\begin{aligned} \theta &= \theta_\alpha = \theta_\gamma = \ell_\alpha = \ell_\gamma, \\ \phi &= \phi_\alpha = \phi_\gamma = \nu_\alpha = \nu_\gamma. \end{aligned} \tag{10}$$

Consequently, the RLM kinetic energy is simpler than Eq. (8), namely,

$$\begin{aligned} T &= \mu/2\left[\dot{R}_\alpha^2 + \dot{r}_\alpha^2 + (R_\alpha^2 + r_\alpha^2)(\dot{\theta}^2 + \sin^2\theta\ \dot{\phi}^2)\right], \\ &= \mu/2\left[\dot{R}_\gamma^2 + \dot{r}_\gamma^2 + (R_\gamma^2 + r_\gamma^2)(\dot{\theta}^2 + \sin^2\theta\ \dot{\phi}^2)\right]. \end{aligned} \tag{11}$$

In natural collision coordinates, the RLM kinetic energy becomes

$$T = \mu/2\left[\eta^2\dot{u}^2 + \dot{v}^2 + \rho^2(\dot{\theta}^2 + \sin^2\theta\ \dot{\phi}^2)\right]. \tag{12}$$

and in hyperspherical coordinates we obtain

$$T = \mu/2\left[\dot{\rho}^2 + \rho^2\dot{\varphi}^2 + \rho^2(\dot{\theta}^2 + \sin^2\theta\ \dot{\phi}^2)\right]. \tag{13}$$

2.3. The Quantum Mechanical Kinetic Energy Operator

To obtain the quantum kinetic energy operator, we first rewrite the classical expression in terms of momenta conjugate to the coordinates, and then follow the prescription described by Podolsky[62] or Margenau and Murphy.[63] In α-channel Jacobi coordinates, we obtain

$$\hat{T}_{RLM} = -\frac{\hbar^2}{2\mu}\left[\frac{1}{\rho^2}\frac{\partial}{\partial R_\alpha}\rho^2\frac{\partial}{\partial R_\alpha} + \frac{1}{\rho^2}\frac{\partial}{\partial r_\alpha}\rho^2\frac{\partial}{\partial r_\alpha}\right] + \frac{\hat{J}^2}{2\mu\rho^2}, \tag{14}$$

where $\hat{J}$ is the total angular momentum operator for the system

$$\hat{J}^2 = -\hbar^2\left[\frac{1}{\sin\theta}\frac{\partial}{\partial\theta}\sin\theta\frac{\partial}{\partial\theta} + \frac{1}{\sin^2\theta}\frac{\partial^2}{\partial\phi^2}\right]. \tag{15}$$

In natural collision coordinates, $\hat{T}$ becomes

$$\hat{T}_{RLM} = -\frac{\hbar^2}{2\mu}\left[\frac{1}{\eta^2\rho^2}\frac{\partial}{\partial u}\rho^2\frac{\partial}{\partial u} + \frac{1}{\eta\rho^2}\frac{\partial}{\partial v}\eta\rho^2\frac{\partial}{\partial v}\right] + \frac{\hat{J}^2}{2\mu\rho^2}, \qquad (16)$$

and in hyperspherical coordinates we obtain

$$\hat{T}_{RLM} = -\frac{\hbar^2}{2\mu}\left[\frac{1}{\rho^3}\frac{\partial}{\partial\rho}\rho^3\frac{\partial}{\partial\rho} + \frac{1}{\rho^2}\frac{\partial^2}{\partial\varphi^2}\right] + \frac{\hat{J}^2}{2\mu\rho^2}. \qquad (17)$$

In the RLM, the Hamiltonian operator is simply

$$\hat{H}_{RLM} = \hat{T}_{RLM} + V_{1D}(R,r), \qquad (18)$$

where $V_{1D}(R,r)$ is the electronic potential energy hypersurface, for collinear geometries. Of course, we assume V_{1D} may be evaluated as needed in any of the required coordinate systems.

2.4. The Bending Hamiltonian

We next elaborate upon the RLM to account approximately for the neglected bending degrees of freedom. Bending is treated as if it is adiabatically separable from motion in the R and r coordinates, as if bending time scales were faster than time scales for translational and vibrational motion. The true time scales associated with these motions almost never satisfy these conditions (especially asymptotically), except for some reactions with highly constrained linear intermediates and at collision energies near the reaction threshold. Nevertheless, we include the bending approximation to improve the threshold behavior of reactions, hoping that in some average sense, it may recover some of the features expected from the internal rotational degrees of freedom in a more accurate 3D theory. However, the two degenerate bending modes correlate to zero-frequency modes asymptotically, and not to the proper diatomic rotational levels. Consequently, we cannot identify the results of a BCRLM calculation for a specific set of bending states with those of a 3D theory for specific rotational transitions. However, as we describe later, we may identify bending averaged[64] BCRLM results with rotationally averaged 3D results.

Following Garrett and Truhlar,[29] we define the angle γ (not to be confused with the arrangement channel index) as the bond angle between the $-\vec{r}_{BC}$ and $\vec{r}_{AB}$ vectors defined by Eq. (2). For small displacements in the γ angle, we may define a bending Hamiltonian for each (R,r) or (ρ,φ)

$$\hat{H}_{bend} = \frac{\hbar^2}{2I_b}\frac{\partial^2}{\partial\gamma^2} + V_{bend}(\gamma;R,r), \qquad (19a)$$

where I_b is a moment of inertia.

$$I_b^{-1} = [m_A R_{AB}^2]^{-1} + [m_C R_{BC}^2]^{-1} + m_B^{-1}[R_{AB}^{-1} + R_{BC}^{-1}]^2. \quad (19b)$$

The eigenvalues of this Hamiltonian are $\epsilon_\lambda(R,r)$,

$$\hat{H}_{bend}\Psi_\lambda^{bend} = \epsilon_\lambda(R,r)\Psi_\lambda^{bend} \quad (20)$$

and form an effective potential which, when added to the collinear potential surface, forms the BCRLM potential. We have therefore

$$V_{\lambda_1\lambda_2}(R,r) = V_{1D}(R,r) + \epsilon_{\lambda_1}(R,r) + \epsilon_{\lambda_2}(R,r), \quad (21)$$

$$\hat{H}_{BCRLM}^{\lambda_1\lambda_2} = \hat{T}_{RLM} + V_{\lambda_1\lambda_2}(R,r). \quad (22)$$

The bending eigenvalue functions appear twice in Eq. (21) because of the degeneracy of the two bending modes of a linear triatomic molecule. In practice, BCRLM calculations have been reported[15,64-71] only for an approximate form of the bending eigenvalue function, and for $\lambda_1=\lambda_2=0$. The approximation used[15] is expressed in natural collision coodinates,

$$\tilde{\epsilon}_\lambda(u,v) = \epsilon_\lambda(u,v_o), \quad (23)$$

where v_o is the value of v where the potential $V_{1D}(u,v)$ has a minimum at fixed u. This approximation has been used for computational convenience but may have several disadvantages. The first problem[15] arises because the approximation is tied to the definition of the natural collision coordinates. This dependency arises because the position of the vibrational minimum v_o depends slightly on the location of TC, and lines of constant u are not perpendicular to the minimum energy path from the saddle point toward reactants (or products). A second problem arises in hyperspherical coordinates, because Eq. (23) becomes quite cumbersome to implement, and indeed, the effective potential becomes multivalued at TC. A third problem arises at subthreshold collision energies, where collinear calculations show that significant corner-cutting of reactive flux occurs to the concave side of the minimum energy path. It has been pointed out[72] that in this region, the approximate potential is likely to be larger than ϵ_λ; consequently, the barrier to tunnelling may be overestimated. The simple solution to each of these problems is to avoid the approximation Eq. (23) altogether.

2.5. The Coupled-Channel Equations

The angular momentum operator in Eq. (15) suggests that the overall rotational degrees of freedom can be expanded in partial waves using spherical harmonics $Y_J^0(\theta,\phi)$, so that

$$\Psi_m^{\lambda_1\lambda_2}(R,r,\theta,\phi) = \sum_{J=0}^{\infty} A_m^J \Psi_m^{J\lambda_1\lambda_2}(R,r)\, Y_J^0(\theta,\phi), \tag{24}$$

where λ_1 and λ_2 label adiabatic bending states, J is the total angular momentum quantum number, and m labels the initial vibrational state. The coefficient A_m^J is chosen to satisfy asymptotic boundary conditions in Sec. 2.8. We next expand the coefficient functions $\Psi_m^{J\lambda_1\lambda_2}(R,r)$ as appropriate for each coordinate system. In Jacobi coordinates, we have

$$\Psi_m^{J\lambda_1\lambda_2}(R,r) = \rho^{-1} \sum_{i=1}^{M} \sum_{n=1}^{N} f_{nm}(R;iJ\lambda_1\lambda_2)\, F_n(r;iJ\lambda_1\lambda_2), \tag{25}$$

and in natural collision coordinates, we have

$$\Psi_m^{J\lambda_1\lambda_2}(R,r) = \rho^{-1}\eta^{1/2} \sum_{i=1}^{M} \sum_{n=1}^{N} g_{nm}(u;iJ\lambda_1\lambda_2)\, G_n(v;iJ\lambda_1\lambda_2), \tag{26}$$

and in hyperspherical coordinates, we have

$$\Psi_m^{J\lambda_1\lambda_2}(R,r) = \rho^{-3/2} \sum_{i=1}^{M} \sum_{n=1}^{N} h_{nm}(\rho;iJ\lambda_1\lambda_2)\, H_n(\varphi;iJ\lambda_1\lambda_2). \tag{27}$$

In Eqs. (25)-(27), we subdivided configuration space into sectors, each labeled by the index i; the boundary between sectors in each coordinate system is formed by curves on which the propagation variables (R, u, and ρ, respectively) are constant. Since the wavefunction expansion may change from sector to sector, the functions f, F, g, G, h, and H depend parametrically on the i index, as well as the total angular momentum index J and the adiabatic bend quantum numbers λ_1 and λ_2.

The functions F, G, and H are determined by solving a reference vibrational Hamiltonian defined at the center of each sector,

$$\left[-\frac{\hbar^2}{2\mu}\frac{d^2}{dr^2} + \tilde{V}_F(r;iJ\lambda_1\lambda_2) - \epsilon_n^F(iJ\lambda_1\lambda_2)\right] F(r;iJ\lambda_1\lambda_2) = 0, \tag{28}$$

$$\left[-\frac{\hbar^2}{2\mu}\frac{d^2}{dv^2} + \tilde{V}_G(v;iJ\lambda_1\lambda_2) - \epsilon_n^G(iJ\lambda_1\lambda_2)\right] G(v;iJ\lambda_1\lambda_2) = 0, \tag{29}$$

$$\left[-\frac{\hbar^2}{2\mu\rho^2}\frac{d^2}{d\varphi^2} + \tilde{V}_H(\varphi;iJ\lambda_1\lambda_2) - \epsilon_n^H(iJ\lambda_1\lambda_2)\right] H(\varphi;iJ\lambda_1\lambda_2) = 0. \tag{30}$$

The actual choice of the reference vibrational potential depends on the particular application. In the RXN1D program,[73] a quadratic reference potential is chosen[49] in the NCC and Jacobi coordinate systems, and the functions F and G form a harmonic oscillator basis. In hyperspherical coordinates, we use the entire potential and determine the basis H by a finite difference approach.

Combining Eqs. (24)-(30) with Eqs. (14)-(18), we obtain the coupled-channel equations for the propagation functions $f_{nm}(R)$, $g_{nm}(u)$, and $h_{nm}(\rho)$, which after suppressing the parametric labels $(iJ\lambda_1\lambda_2)$ are,

$$\frac{d^2}{dR^2} f_{nm}(R) = \sum_{n'=0}^{N} (\underline{\underline{D}}_F)_{nn'} f_{n'm}(R), \tag{31}$$

$$\frac{d^2}{du^2} g_{nm}(u) = \sum_{n'=0}^{N} (\underline{\underline{D}}_G)_{nn'} g_{n'm}(u), \tag{32}$$

$$\frac{d^2}{d\rho^2} h_{nm}(\rho) = \sum_{n'=0}^{N} (\underline{\underline{D}}_H)_{nn'} h_{n'm}(\rho), \tag{33}$$

where in Eqs. (31)-(33) the coupling matrices (we denote matrices by a double underline) are

$$\frac{\hbar^2}{2\mu} (\underline{\underline{D}}_F)_{nn'} = (\epsilon_n - E)\delta_{nn'} + \langle F_n | V_{\lambda_1\lambda_2} - \tilde{V}_F + \frac{\hbar^2}{2\mu\rho^2}[J(J+1)+1] | F_{n'} \rangle, \tag{34}$$

$$\frac{\hbar^2}{2\mu} (\underline{\underline{D}}_G)_{nn'} = \frac{3}{4\sigma^2}\delta_{nn'} + \langle G_n | \eta^2 \left\{ V_{\lambda_1\lambda_2} - \tilde{V}_G + \frac{(\epsilon_n + \epsilon_{n'})}{2} - E + \frac{\hbar^2}{2\mu\rho^2}[J(J+1)+1] \right\} | G_{n'} \rangle, \tag{35}$$

$$\frac{\hbar^2}{2\mu} (\underline{\underline{D}}_H)_{nn'} = \left[\epsilon_n - E + \frac{\hbar^2}{2\mu\rho^2}\left[J(J+1) + \frac{3}{4} \right] \right]\delta_{nn'} + \langle H_n | V - \tilde{V}_H | H_{n'} \rangle. \tag{36}$$

When we change the target basis (Eqs. (28)-(30)) between two adjacent sectors, we must ensure that the wavefunction and its derivative are

continuous across the sector boundary. Enforcing this requirement defines overlap matrices $\underline{\sigma}$ in each coordinate system, and for Jacobi coordinates we obtain

$$f_{nm}(R_i^+;i) = \sum_{n'} [\underline{\sigma}_F(i,i+1)]_{nn'} f_{n'm}(R_{i+1}^-;i+1), \tag{37}$$

$$[\underline{\sigma}_F(i,i+1)]_{nn'} = \langle F_n(r;i) | F_{n'}(r;i+1) \rangle, \tag{38}$$

where we have suppressed the labels $(J\lambda_1\lambda_2)$ on the f's, F's, and T's. In Eq. (37), R_i^- and R_i^+ are the values of the propagation coordinate at the inner and outer boundaries of sector i. Equations analagous to Eqs. (37)-(38) also hold in the NCC and hyperspherical coordinate systems.

2.6. Solving the Coupled-Channel Equations

The coupled-channel equations (Eq. (31), (32), or (33)), may be solved in a variety of ways, but we use the R-matrix propagation method of Light and Walker.[49,74-76] We will review this method briefly in this section, as applied to the coupled-channel equations in Jacobi coordinates. The approach is essentially the same in other coordinates. The coupling matrices $\underline{D}$ (Eqs. (34)-(36)) are evaluated at the center of each sector, and are assumed to be constant across the sector. The real symmetric $\underline{D}$ matrices are diagonalized by a real orthogonal matrix $\underline{U}$,

$$\underline{U}^T(i) \cdot \underline{D}(i) \cdot \underline{U}(i) = \underline{\lambda}^2(i), \tag{39}$$

where $\underline{U}^T$ is the transpose of $\underline{U}$. The matrix $\underline{U}$ transforms to a locally uncoupled representation, and defines new propagation functions $\tilde{f}_{nm}(R;i)$ in each sector,

$$\underline{\tilde{f}}(R;i) = \underline{U}(i) \cdot \underline{f}(R;i). \tag{40}$$

The global R matrix, between the initial sector and sector i, is

$$\begin{bmatrix} \underline{\tilde{f}}(R_0^-;0) \\ \underline{\tilde{f}}(R_i^+;i) \end{bmatrix} = \begin{bmatrix} \underline{R}_1(i) & \underline{R}_2(i) \\ \underline{R}_3(i) & \underline{R}_4(i) \end{bmatrix} \begin{bmatrix} -\underline{\tilde{f}}'(R_0^-;0) \\ \underline{\tilde{f}}'(R_i^+;i) \end{bmatrix}. \tag{41}$$

The sector R matrix relating the values of the locally uncoupled functions to derivatives within sector (i+1) is

$$\begin{bmatrix} \underline{\tilde{f}}(R_{i+1}^-;i+1) \\ \underline{\tilde{f}}(R_{i+1}^+;i+1) \end{bmatrix} = \begin{bmatrix} \underline{r}_1(i+1) & \underline{r}_2(i+1) \\ \underline{r}_3(i+1) & \underline{r}_4(i+1) \end{bmatrix} \begin{bmatrix} -\underline{\tilde{f}}'(R_{i+1}^-;i+1) \\ \underline{\tilde{f}}'(R_{i+1}^+;i+1) \end{bmatrix}, \tag{42}$$

where for open channels ($\lambda^2 \leq 0$) we have

$$[\underline{r}_1(i)]_{nn'} = [\underline{r}_4(i)]_{nn'} = \delta_{nn'}\left[-|\lambda_n(i)|^{-1}\cot\{\Delta R_i|\lambda_n(i)|\}\right],$$
$$[\underline{r}_2(i)]_{nn'} = [\underline{r}_3(i)]_{nn'} = \delta_{nn'}\left[-|\lambda_n(i)|^{-1}\csc\{\Delta R_i|\lambda_n(i)|\}\right], \tag{43}$$

and for closed channels ($\lambda^2 \geq 0$) the sector R matrix is

$$[\underline{r}_1(i)]_{nn'} = [\underline{r}_4(i)]_{nn'} = \delta_{nn'}\left[|\lambda_n(i)|^{-1}\coth\{\Delta R_i|\lambda_n(i)|\}\right],$$
$$[\underline{r}_2(i)]_{nn'} = [\underline{r}_3(i)]_{nn'} = \delta_{nn'}\left[|\lambda_n(i)|^{-1}\mathrm{csch}\{\Delta R_i|\lambda_n(i)|\}\right]. \tag{44}$$

In Eqs. (43)-(44), ΔR_i is the width of sector i. The transformation matrix from the locally uncoupled representation of sector i to the locally uncoupled representation of sector i+1 is

$$\underline{T}(i,i+1) = \underline{U}^T(i)\cdot\underline{\sigma}(i,i+1)\cdot\underline{U}(i+1). \tag{45}$$

Assuming we know the global R matrix of Eq. (41), we can now compute the global R matrix for sector i+1 using the sector R matrix of Eq. (42) and the overlap matrix of Eq. (45). The R-matrix recursion relations are[77]

$$\underline{R}_1(i+1) = \underline{R}_1(i) - \underline{R}_2(i)\cdot\underline{T}(i,i+1)\cdot\underline{Z}(i+1)\cdot\underline{T}^T(i,i+1)\cdot\underline{R}_3(i), \tag{46}$$

$$\underline{R}_2(i+1) = \underline{R}_3^T(i+1) = \underline{R}_2(i)\cdot\underline{T}(i,i+1)\cdot\underline{Z}(i+1)\cdot\underline{r}_2(i+1), \tag{47}$$

$$\underline{R}_4(i+1) = \underline{r}_4(i+1) - \underline{r}_3(i+1)\cdot\underline{Z}(i+1)\cdot\underline{r}_2(i+1), \tag{48}$$

$$\underline{Z}(i+1) = [\underline{r}_1(i+1) - \underline{T}^T(i,i+1)\cdot\underline{R}_4(i)\cdot\underline{T}(i,i+1)]^{-1}. \tag{49}$$

By repeatedly applying Eqs. (46)-(49), the coupled-channel equations are solved by propagating towards asymptotic regions of configuration space. We also note[76] that, if desired, we may propagate the R-matrix inverse (the log-derivative or L matrix) with equations essentially the same as Eqs. (46)-(49), where only the definition of the sector L matrix is changed. At the conclusion of the propagation, we compute the scattering matrix $\underline{S}$ by enforcing boundary conditions.

In the RXNID program,[73] both the NCC and Jacobi coordinate systems are used. We begin at the collinear matching surface (M in Fig. 1) with a sector R matrix as the first "global" R matrix, and propagate all four blocks of the R matrix outwards toward the α-channel asymptotic region, and then switch to α-Jacobi coordinates when $R_\alpha = R_\alpha^*$. For asymmetric systems ($m_A \neq m_C$), propagation resumes at the matching surface, and proceeds toward the γ-channel asymptotic region, switching to γ-Jacobi coordinates when $R_\gamma = R_\gamma^*$. The α- and γ-channel R matrices are then combined and boundary conditions enforced.

In hyperspherical coordinates, propagation begins at a small hyperspherical radius, and continues to larger hyperspherical radii. Because the potential is repulsive at small radii, only regular functions at the origin are physically allowed, and in this case it is necessary to propagate only the $\underline{R}_{11}$ block of the R matrix. As ρ increases, the angular potential evolves from a single well to a double well, one each for the reactant and product molecules. At energies below dissociation, the barrier between the two wells becomes large and broad enough that the eigenstates of the angular potential are completely localized within each well. For symmetric systems ($m_A=m_C$), we may obtain degenerate pairs of delocalized functions, but these are easily localized (i.e., $\Psi(\text{local}) = 2^{-1/2}[\Psi_1 \pm \Psi_2]$). Once the angular eigenstates are localized, we may continue propagating in Jacobi coordinates, or if appropriate, we may enforce boundary conditions. However, in either case we first project the hyperspherical solutions onto constant R_α (and R_γ) surfaces.

2.7. Hyperspherical Projection

Asymptotic boundary conditions are most conveniently expressed in Jacobi coordinates, and so if we solve the coupled-channel equations in hyperspherical coordinates, we first express our solutions, defined on a hyperspherical radius, on the appropriate Jacobi surfaces (see Fig. 2).

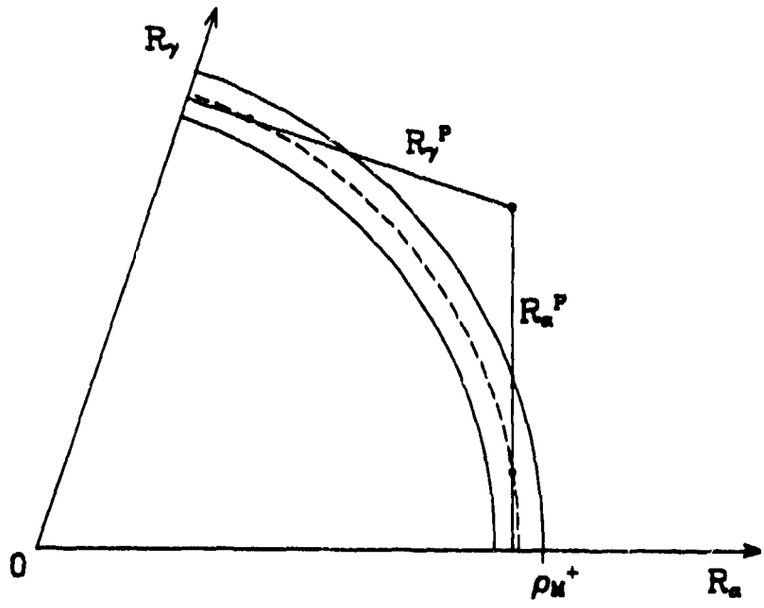

Figure 2. Collinear configuration space, showing the projection of hyperspherical solutions onto Jacobi surfaces. The solid arcs are the inner and outer boundaries of the last hyperspherical sector, and the dashed arc is the center of the sector. The Jacobi surfaces R_α^P and R_γ^P intersect the dashed arc at the vibrational minima.

We describe in this section a procedure which determines a two-surface R matrix (four blocks) from the single surface hyperspherical R matrix. The procedure we describe is essentially that of Bondi and Connor,[48,49] except for minor differences in strategy (they evaluate asymptotic boundary conditions directly on the final hyperspherical radius). We begin by recalling the definition of the final hyperspherical R matrix,

$$\underline{h}(\rho_M^+;M) = \underline{R}^H \cdot \underline{h}'(\rho_M^+;M), \tag{50}$$

where here M labels the final hyperspherical sector (see Eq. (27)), and ρ_M^+ is the value of ρ at the outer boundary of this sector. Within the last sector, the propagation functions (and their derivatives) may be expanded in sine- and cosine-like solutions, so that

$$\underline{h}(\rho;M) = \underline{s}(\rho;M) \cdot \underline{A}_M + \underline{c}(\rho;M) \cdot \underline{B}_M, \qquad \rho_M^- \le \rho \le \rho_M^+, \tag{51}$$

$$\underline{h}'(\rho;M) = \underline{s}'(\rho;M) \cdot \underline{A}_M + \underline{c}'(\rho;M) \cdot \underline{B}_M, \qquad \rho_M^- \le \rho \le \rho_M^+, \tag{52}$$

where $\underline{A}_M$ and $\underline{B}_M$ are undetermined coefficient matrices, constant within the final sector, which depend on asymptotic boundary conditions. The diagonal matrices $\underline{s}(\rho;M)$ and $\underline{c}(\rho;M)$ are

$$\begin{aligned} s_n(\rho) &= \sin[k_n^M(\rho-\rho_M)], && \text{channel n open,} \\ &= \sinh[k_n^M(\rho-\rho_M)], && \text{channel n closed,} \end{aligned} \tag{53}$$

$$\begin{aligned} c_n(\rho) &= \cos[k_n^M(\rho-\rho_M)], && \text{channel n open,} \\ &= \cosh[k_n^M(\rho-\rho_M)], && \text{channel n closed,} \end{aligned} \tag{54}$$

where ρ_M is the value of ρ at the center of the final sector, and

$$\left[k_n^M\right]^2 = |(\underline{D}_H)_{nn}|. \tag{55}$$

By substituting Eqs. (51) and (52) into Eq. (50), we can relate the coefficient matrices $\underline{A}$ and $\underline{B}$,

$$\begin{aligned} \underline{A}_M &= \underline{X}_M \cdot \underline{B}_M, \\ \underline{X}_M &= [\underline{s}(\rho_M^+) - \underline{R}^H \cdot \underline{s}'(\rho_M^+)]^{-1} \cdot [\underline{c}(\rho_M^+) - \underline{R}^H \cdot \underline{c}'(\rho_M^+)]. \end{aligned} \tag{56}$$

We now require the right hand sides of Eqs. (25) and (27) to agree on the projection surface $R_\alpha = R_\alpha^P$ (see Fig. 2),

$$\rho^{-1/2} \sum_{n'} h_{n',m}(\rho;M)\, H_{n',}(P;M) = \sum_{n} f_{nm}(R_\alpha^P)\, F_n(r_\alpha), \tag{57}$$

and a similar equation must also hold for the derivatives

$$\frac{\partial}{\partial R_\alpha}\left[\rho^{-1/2} \sum_{n'} h_{n',m}(\rho;M)\, H_{n',}(P;M)\right] = \sum_{n} f'_{nm}(R_\alpha^P)\, F_n(r_\alpha). \tag{58}$$

Two additional equations, similar to Eqs. (57) and (58), also hold on the product surface R_γ^P. We next multiply by $F_n^*(r_\alpha)$ and integrate over r_α (and over r_γ on the product surface), and use Eqs. (51) and (52) to obtain equations for the propagation functions in Jacobi coordinates.

$$\begin{bmatrix} \underline{f}(R_\alpha^P) \\ \underline{f}(R_\gamma^P) \end{bmatrix} = \begin{bmatrix} \underline{I}_\alpha^{(1)} & \underline{0} \\ \underline{0} & \underline{I}_\gamma^{(1)} \end{bmatrix} \cdot \underline{A}_M + \begin{bmatrix} \underline{I}_\alpha^{(2)} & \underline{0} \\ \underline{0} & \underline{I}_\gamma^{(2)} \end{bmatrix} \cdot \underline{B}_M, \tag{59}$$

$$\begin{bmatrix} \underline{f}'(R_\alpha^P) \\ \underline{f}'(R_\gamma^P) \end{bmatrix} = \begin{bmatrix} \underline{I}_\alpha^{(3)} & \underline{0} \\ \underline{0} & \underline{I}_\gamma^{(3)} \end{bmatrix} \cdot \underline{A}_M + \begin{bmatrix} \underline{I}_\alpha^{(4)} & \underline{0} \\ \underline{0} & \underline{I}_\gamma^{(4)} \end{bmatrix} \cdot \underline{B}_M, \tag{60}$$

where the α-channel matching matrices are defined (suppressing the M label on the s, c, and H functions)

$$\left[\underline{I}_\alpha^{(1)}\right]_{nn'} = \int_0^\infty F_n(r_\alpha)\, \rho^{-1/2}\, s_{n',}(\rho)\, H_{n',}(P)\, dr_\alpha, \tag{61}$$

$$\left[\underline{I}_\alpha^{(2)}\right]_{nn'} = \int_0^\infty F_n(r_\alpha)\, \rho^{-1/2}\, c_{n',}(\rho)\, H_{n',}(P)\, dr_\alpha, \tag{62}$$

$$\begin{aligned}\left[\underline{I}_\alpha^{(3)}\right]_{nn'} = \int_0^\infty F_n(r_\alpha)\, \rho^{-1/2} &(s'_{n',}(\rho)\, H_{n',}(P)\cos P - \\ &- (2\rho)^{-1}\, s_{n',}(\rho)\, H_{n',}(P)\cos P \\ &- \rho^{-1}\, s_{n',}(\rho)\, H'_{n',}(P)\sin P)\, dr_\alpha,\end{aligned} \tag{63}$$

$$\begin{aligned}\left[\underline{I}_\alpha^{(4)}\right]_{nn'} = \int_0^\infty F_n(r_\alpha)\, \rho^{-1/2} &(c'_{n',}(\rho)\, H_{n',}(P)\cos P - \\ &- (2\rho)^{-1}\, c_{n',}(\rho)\, H_{n',}(P)\cos P \\ &- \rho^{-1}\, c_{n',}(\rho)\, H'_{n',}(P)\sin P)\, dr_\alpha.\end{aligned} \tag{64}$$

The off-diagonal blocks of the $\underline{I}^{(1)}$, $\underline{I}^{(2)}$, $\underline{I}^{(3)}$ and $\underline{I}^{(4)}$ matrices in Eqs. (59)-(60) are zero because we have assumed that the hyperspherical angular eigenfunctions have been localized in the reactant and product potential wells. Referring back to Eq. (41), we can define an R matrix for the Jacobi coordinates

$$\begin{bmatrix} \underline{f}(R_\alpha^P) \\ \underline{f}(R_\gamma^P) \end{bmatrix} = \begin{bmatrix} \underline{R}_1^F & \underline{R}_2^F \\ \underline{R}_3^F & \underline{R}_4^F \end{bmatrix} \begin{bmatrix} \underline{f}'(R_\alpha^P) \\ \underline{f}'(R_\gamma^P) \end{bmatrix}. \tag{65}$$

Combining Eqs. (59) and (60) with Eqs. (56) and (65), the Jacobi R matrix is determined in terms of the matching matrices as

$$\underline{R}^F = \left[\underline{I}^{(1)} \cdot \underline{X}_M + \underline{I}^{(2)} \right] \cdot \left[\underline{I}^{(3)} \cdot \underline{X}_M + \underline{I}^{(4)} \right]^{-1} \tag{66}$$

where in Eq. (66) we have implicitly arranged the rows and columns of $\underline{X}$ to agree with the labeling implied by Eqs. (59)-(60). Having determined the R matrix in Jacobi coordinates, we can now either continue the propagation or apply asymptotic boundary conditions.

2.E. Boundary Conditions

The coupled-channel equations (Eqs. (31) and (34)) decouple at large values of R_α (or R_γ), because in the limit that $\rho \to R$, we obtain

$$\frac{\hbar^2}{2\mu} (\underline{D}_F)_{nn'} = \left[\epsilon_n - E + \frac{\hbar^2}{2\mu R^2} [J(J+1)+1] \right] \delta_{nn'} . \tag{67}$$

The form of Eq. (67) implies that the functions $f_{nm}(R;J)$ will approach a linear combination of Bessel functions of unusual order, because of the $J(J+1)+1$ term. In our calculations, we have ignored the additional $1/R^2$ centrifugal potential in applying boundary conditions, in order to use the more familiar spherical Bessel functions. Our experience has been, and others have shown,[70] that this approximation has a small effect on the magnitudes and phases of the final S-matrix elements. We therefore require the functions $f_{nm}(R;J)$ to go asymptotically[9] as

$$f_{nm}(R;J) \sim -ik_n R \left[\mathcal{A}_J^{(1)}(k_n R)\delta_{nm} + \mathcal{A}_J^{(1)}(k_n R) \, (k_m/k_n)^{-1/2} S_{nm}^J \right], \tag{68}$$

where k_n is the channel wavenumber $\hbar^2 k_n^2 = 2\mu(E-\epsilon_n)$, S_{nm}^J is an element of the S matrix, and the functions $\mathcal{A}_J$ are spherical Hankel functions of the first and second kind, which themselves have the asymptotic behavior

$$\pm i\mathcal{A}_J^{(1),(2)}(z) \to z^{-1} \exp[\pm i(z - J\pi/2)]. \tag{69}$$

The wavefunction of Eq. (24) must satisfy the boundary condition[9]

$$\Psi_m^{\lambda_1\lambda_2}(R,r,\theta,\phi) \sim F_m^{\infty}(r_\alpha)\exp[ik_m R_\alpha \cos\theta_\alpha] +$$

$$+ R_\alpha^{-1} \sum_n \exp[ik_n R_\alpha]\ F_n^{\infty}(r_\alpha)\ \mathcal{A}_{nm}(\theta,\phi), \qquad (70)$$

when R_α is large,

$$\sim R_\gamma^{-1} \sum_{n'} \exp[ik_{n'} R_\gamma]\ F_{n'}^{\infty}(r_\gamma)\ \mathcal{A}_{n'm}(\theta,\phi), \qquad (71)$$

when R_γ is large.

In Eqs. (70)-(71), the functions $F^{\infty}(r)$ are the eigenfunctions of the asymptotic vibrational Hamiltonian, and $\mathcal{A}(\theta,\phi)$ is the scattering amplitude. Using the asymptotic form of f_{nm} defined in Eqs. (68) and (69) in the right-hand-side of Eq. (24), we determine the expansion coefficients A_m^J in Eq. (21) and the scattering amplitude $\mathcal{A}_{nm}$ by equating with Eqs. (70) and (71). The coefficients A_m^J are determined by equating the coefficients of the incoming spherical waves, obtaining

$$A_m^J = k_m^{-1}\ i^{J+1}\ [\pi(2J+1)]^{1/2} \qquad (72)$$

The scattering amplitude is similarly determined by equating the coefficients of the outgoing spherical waves, after first expanding $\mathcal{A}_{nm}$ in Legendre polynomials. We obtain[9]

$$\mathcal{A}_{nm}(\theta,\phi) = i(4k_n k_m)^{-1/2} \sum_{J=0}^{\infty} (2J+1)\ (\delta_{nm} - S_{nm}^J)\ P_J(\cos\theta). \qquad (73)$$

The calculation of the S matrix from the final R matrix is accomplished by rewriting Eq. (68) and its derivative in matrix form,

$$\underline{f}(R;J) = \underline{\mathcal{J}}(J) - \underline{\mathcal{O}}(J)\cdot\underline{k}^{-1/2}\cdot\underline{S}^J\cdot\underline{k}^{1/2}, \qquad (74)$$

$$\underline{f}'(R;J) = \underline{\mathcal{J}}'(J) - \underline{\mathcal{O}}'(J)\cdot\underline{k}^{-1/2}\cdot\underline{S}^J\cdot\underline{k}^{1/2}, \qquad (75)$$

where $\underline{f}(R)$ and $\underline{f}'(R)$ are matrices of the values of the propagation functions and their derivatives on the final R-matrix boundaries in both the α and γ arrangement channels. Here the diagonal $\underline{\mathcal{J}}$ and $\underline{\mathcal{O}}$ matrices (and their derivatives) are the spherical Hankel functions of Eq. (68).

$$[\underline{\sigma}(J)]_{nn} = ik_n R\, \mathcal{A}_J^{(1)}(k_n R), \tag{76}$$

$$[\underline{\sigma}'(J)]_{nn} = [\underline{\sigma}(J)]^*_{nn}, \tag{77}$$

where * denotes the complex conjugate. The $\underline{\sigma}$ matrix defined here should not be confused with the overlap matrix used in Eqs. (37), (38), and (45). Defining the final R matrix as $\underline{R}^{\infty}$, and combining the definition of the R matrix (see Eq. (65)) with Eqs. (74)-(75), the S matrix is

$$\underline{S}^J = \underline{k}^{1/2} \cdot \left[\underline{\sigma}(J) - \underline{R}^{\infty} \cdot \underline{\sigma}'(J)\right]^{-1} \cdot \left[\underline{\sigma}(J) - \underline{R}^{\infty} \cdot \underline{\sigma}'(J)\right]^* \cdot \underline{k}^{-1/2} \tag{78}$$

2.9. Differential and Integral Cross Sections, Thermal Rate Constants

The differential scattering cross section in the RLM is defined as usual, the ratio of the spherically scattered flux into final state n originating from an incident plane wave in molecular state m,

$$\frac{d}{d\Omega}\sigma_{nm}(\theta,\phi;E) = (k_n/k_m)\, |\mathcal{A}_{nm}(\theta,\phi)|^2, \tag{79}$$

where $\mathcal{A}_{nm}(\theta,\phi)$ is defined in Eq. (73). The integral cross section is obtained by integrating over the polar angles, giving the familiar form

$$\sigma_{nm}(E) = \pi k_m^{-2} \sum_{J=0}^{\infty} (2J+1)\, |\delta_{nm} - S^J_{nm}|^2. \tag{80}$$

From the integral cross section we can compute a state-to-state thermal rate constant in the standard way,[78]

$$K_{nm}(T) = N\, (2/k_B T)^{3/2}\, (\pi \mu_{A,BC})^{-1/2} \times$$

$$\times \int_0^{\infty} E_t\, \sigma_{nm}(E_t + \epsilon_m)\, \exp[-E_t/k_B T]\, dE_t, \tag{81}$$

where N is Avogadro's number, k_B is Boltzmann's constant, E_t is the initial translational energy of reactants in vibrational state m, and $\mu_{A,BC}$ is the reduced mass of the initial collision partners.

$$\mu_{A,BC} = m_A(m_B + m_C)/(m_A + m_B + m_C). \tag{82}$$

Definitions similar to Eqs. (79)-(81) also hold for differential cross sections, integral cross sections, and rate constants in the BCRLM, except that each is obtained for every choice of bending states λ_1 and λ_2.

2.10. The Relationship between RLM/BCRLM and 3D -- Rotational Averaging

Although cross sections and rate constants in the RLM are well defined quantities, it is nevertheless difficult to compare directly to full three-dimensional calculations because the RLM neglects internal bending and rotational degrees of freedom. Philosophically, it is better to ask how one should sum or average the results of full 3D calculations in order to obtain quantities which best compare with the models. Since in the RLM or BCRLM, the diatomics do not rotate before or after the collision, we may be tempted to compare 3D $(n,j=0) \rightarrow (n',j'=0)$ processes with RLM $n \rightarrow n'$ processes. In cases where such comparisons can be made, the RLM probabilities, cross sections, and rate constants are larger than the corresponding 3D quantities at all energies and temperatures. The comparison is improved for 3D processes from $(n,j=0)$ to (n',all j'); but even here, RLM results are too large, especially at reaction thresholds, where at least for the cases where detailed 3D results are available,[6-8,13] threshold behavior is strongly influenced by the bending zero point energy of the collision complex in the strong interaction region (i.e., the transition state). It is this latter effect which we address to some extent by augmenting the RLM with a bending Hamiltonian.

The inclusion of effective potentials into the BCRLM in order to account approximately for the neglected bending degrees of freedom in the RLM should make it possible to compare more directly with 3D calculations. Such comparisons are difficult because bending motion is relevant only when the collision partners are close together, and not asymptotically, where boundary conditions are imposed and where the angular motion becomes that of a free rotor. Although the lowest bending states $\lambda_1=\lambda_2=0$ do correllate with the lowest free rotor states $j=j'=0$, we cannot generally define a mapping between higher bending states and higher free rotor states. Consequently, comparisons between BCRLM and full 3D calculations require that we average both sets of results.[64,79] In the BCRLM, we average over the bending degrees of freedom labelled by λ_1 and λ_2, and compare to 3D calculations averaged over the analogous rotational degrees of freedom j, j', l, and l', where l is a label for orbital angular momentum.

The appropriate kind of rotational averaging has been discussed for several years by Bowman and coworkers,[10-14] in connection with a hierarchy of dimensionality reducing theories of reactions. Although the BCRLM differs in origin from these dimensionality reducing theories, it resembles them in spirit, and in detail at some levels. Specifically, the application of microcanonical rotational averaging to BCRLM has been presented by Walker and Pollak,[64] and we will review only the final results here.

In this section, we use square brackets ([]) to indicate quantities which have been microcanonically summed, braces ({}) to indicate quantities which have been microcanonically averaged, and angle brackets (<>) to indicate quantities which have been thermally averaged. The appropriate 3D microcanonically averaged rotational cross section with which we wish to compare is[64,80]

$$(\sigma_{nm}(E)) = \pi\,[\mathcal{P}_{nm}(E)] \,/\, [k_m^2], \tag{83}$$

where $[k_m^2]$ is a cumulative translational wavenumber for reactants,

$$[k_m^2] = 2\mu_{A,BC}\hbar^{-2} \sum_{j=0}^{\infty} (2j+1)\ (E-\epsilon_{mj})\ \Theta(E-\epsilon_{mj}), \tag{84}$$

and ϵ_{mj} is the internal energy of the initial molecule in vibrational state m and rotational state j. The Heaviside function $\Theta(x)$ in Eq. (84) indicates that the summation runs over only open channels at total energy E. In Eq. (83), $[\mathcal{P}_{nm}(E)]$ is a cumulative rotational probability, which for a full 3D calculation is defined as

$$[\mathcal{P}_{nm}(E)] = \sum_{J=0}^{\infty} (2J+1) \sum_{j,j'=0}^{\infty} \sum_{l,l'} P^{J}_{nj'l'mjl}(E-\epsilon_{mj}), \tag{85}$$

where the sums over l and l' run over the triangle inequality with J and j (or j'), and $P^{J}_{nj'l'mjl}$ is the reaction probability, the absolute square of an element of the 3D S matrix.

In the BCRLM, the cumulative reaction probability is one in which we sum over the bending degrees of freedom, approximating Eq. (85) as

$$[\mathcal{P}_{nm}(E)] = \mathcal{A} \sum_{\lambda=0}^{\infty} \sum_{\Lambda=-\lambda}^{\lambda}{}_{2} \sum_{J=|\Lambda|}^{\infty} (2J+1)\ P^{J\lambda_1\lambda_2}_{nm}(E), \tag{86}$$

where λ is a principal bending quantum number ($\lambda = \lambda_1+\lambda_2$), Λ is an internal bending angular momentum ($\Lambda = \lambda_1-\lambda_2$), and the notation Σ_2 indicates that the summation over Λ goes in steps of two. The reaction path multiplicity factor $\mathcal{A}$ in Eq. (86) assumes values of one or two, the latter for the case of an initial homonuclear diatomic. In practice,[64] we have further approximated Eq. (86) by writing reaction probabilities for higher bending states in terms of those for the lowest bending state, using transition state theory arguments.[19,24]

Given the cumulative reaction probabilities, we can compute thermally averaged rate constants,

$$K_{nm}(T) = \hbar^2 N (2\pi)^{1/2} (\mu_{A,BC} k_B T)^{-3/2}\ \langle \mathcal{P}_{nm}(E) \rangle \,/\, Q_m(T), \tag{87}$$

where Q_m is the rotational partition function

$$Q_m(T) = \sum_{j=0}^{\infty} (2j+1)\ \exp(-\epsilon_{mj}/k_B T), \tag{88}$$

and the thermal average of the cumulative reaction probability is

$$\langle \mathcal{P}_{nm}(E) \rangle = \int_0^\infty \exp(-E/k_B T)\, [\mathcal{P}_{nm}(E)]\, dE. \qquad (88)$$

3. REVIEW OF APPLICATIONS OF THE BCRLM

To date, the BCRLM has been applied to a handful of chemically reactive systems, namely the hydrogen exchange reaction H + H_2 and its isotopic counterparts,[18,64,65] and to the F + H_2 reaction and its isotopic counterparts.[66-69] Some preliminary results have also been presented[67] for the ^{3}He + H_2^+ reaction as well. Lagana'[71] has extended the calculations for the H+H_2 reaction to higher collision energies, and de Haar, Balint-Kurti, and Wyatt[70] have considered the H + Cl_2 reaction. We have already discussed in the previous section an extension[64] of the BCRLM in which we define averaged cross sections and rate constants; when applied to the D+H_2(m=0,1) reaction, we obtained an excellent comparison with shifted sudden calculations of Abu-Salbi, Kouri, Shima, and Baer.[91,92]

The primary concern of the first BCRLM paper[18] was to investigate the extent to which the 300K rate constants (RLM and BCRLM) for the reactions H + H_2(m=1) and D + H_2(m=1) are determined by collisions at energies below the height of the adiabatic reaction barrier. The rate constants determined were compared to experiment[93,94] and to a classical trajectory calculation,[95] but since they are not rotationally averaged, these rates are certainly an upper limit to the true rates on the potential surface[96,97] we used.

Our interest turned then to the relationship between scattering resonances and the angular distribution (differential cross section) predicted by the BCRLM. We showed[68] that for both reactions mentioned above, the angular distribution moves from backwards peaked at low collision energies to more sideways peaked at higher energies, even though the reaction dynamics at threshold is dominated in the H+H_2(m=1) case by a resonance and no resonance appears in the D+H_2(m=1) case. Our interest in this relationship was sparked by the F+H_2 reaction, which also shows[98-99] a shift in the angular distribution, and has a definite threshold resonance contribution. We therefore analyzed[66] the BCRLM angular distribution for the F+H_2 reaction, and concluded that while the presence of a threshold resonance does contribute to the sideways shift in the angular distribution, it is probably not the only source of the feature. Pursuing this idea further, we attempted to separate the resonant and background contributions to the angular distribution in a following paper,[67] using isolated narrow resonance approximations.

We have also used the BCRLM as a tool to investigate the relationship between parameters which define potential energy surfaces

and dynamic features such as resonances, angular distributions,[68] and the position of reaction thresholds.[69] This work has concentrated on the $F+D_2$ reaction, and has aided the development of improved potential energy surfaces.[69,96]

4. EXTENSIONS AND FURTHER APPLICATIONS OF THE METHOD

There is currently work in progress which will extend some of the ideas of the BCRLM either to improve the quantitative reliability of the method, or to enlarge the range of problems to which it is applicable.

4.1. Hybrid Sudden and Adiabatic Methods

As is evidenced by recent literature[97-100] and in other contributions in this volume, there is considerable interest in understanding the nature of the rotation-bending dynamics of reactions in the energy regime near the reaction threshold. For many reactions, and perhaps for most reactions, the dynamics of bending motion at threshold is adiabatic, but above threshold energies, the motion seems to switch over to a sudden type of behavior.[99] Consequently, work in progress[100-1] would define a hybrid sudden-adiabatic theory which would produce reaction cross sections in agreement with adiabatic thresholds (e.g., BCRLM) and in agreement with reactive sudden cross sections[91-2,102-3] at higher collision energies. If this work proves fruitful, and we learn how to model the crossover between adiabatic and sudden reaction dynamics, then we may hope to considerably improve the predictive nature of approximate theories of reactions.

4.2. Non-collinearly Dominated Reactions

The BCRLM is by its very nature constrained to treating collinearly dominated reaction processes. One could extend the method to non-collinear systems by including effective potential terms and more complicated kinetic energy operators to represent the motion of the reacting system along its (bent) minimum energy path from reactants to products. This is indeed an example of the Carrington and Miller[93] reaction surface Hamiltonian theory, which at present is probably the most fruitful approach for noncollinear systems.

4.3. Coupling the Bending Degrees of Freedom

A fairly straightforward extension of the method would be to include the coupling between the lowest and higher bending degrees of freedom while solving the coupled-channel equations. Such an approach may have the beneficial effect of lowering the overall reactivity characteristic of the BCRLM at post-threshold energies, since inelastic bending transitions may reflect otherwise reactive flux prior to reaching the reaction barrier. Unfortunately, there is no significance to individual

bend-state to bend-state cross sections, because bend states have no well defined asymptotic meaning; we would therefore still need to rotationally average (i.e., bending average) our results. Furthermore, any improvements would come at the cost of substantially increasing the computer requirements of the method, to a level comparable to 3D centrifugal sudden (CS) reactive calculations. If such a level of computer effort is available, it would therefore seem appropriate to do the 3D CS calculation instead.

4.4. Photodissociation of Linear Triatomics

A promising extension of the BCRLM to new problems lies in the photodissociation of some triatomics. The application of quantum half-scattering methods to problems of photodissociation is well known,[104-8] and for molecules whose ground and excited electronic surfaces are linearly dominated, the approximations inherent in BCRLM are quite appropriate. To treat photodissociation, we must compute the overlap of the scattering wavefunction on the excited electronic surface with the initial bound state wavefunction on the ground surface. Methods for computing the required overlaps as the R-matrix solution of the coupled-channel equations progresses have been described by Kulander and Light[106] and by Schneider and Taylor.[108] In addition to its relevance to photodissociation, these techniques provide a way to recover the scattering wavefunction from an R-matrix calculation, since the "bound state" wavefunction can be a delta function or a narrow gaussian. The technique for accumulating these overlaps resembles the hyperspherical-to-Jacobi projection described earlier, and so we will review it here.

Using the Jacobi coordinate system as an example, we seek the overlap $\mathfrak{X}_{nm}$ of the scattering wavefunction Ψ_m in Eq. (24) with a bounded function $\mathfrak{F}_n(R,r)$. We begin by expanding the propagation functions in each sector with sine- and cosine-like functions,

$$\begin{aligned}
s_n(R;i) &= \sin[k_n^i(R-R_i^+)], && \text{channel n open,}\\
s_n(R;i) &= \sinh[k_n^i(R-R_i^+)], && \text{channel n closed,}\\
c_n(R;i) &= \cos[k_n^i(R-R_i^+)], && \text{channel n open,}\\
c_n(R;i) &= \cosh[k_n^i(R-R_i^+)], && \text{channel n closed,}
\end{aligned} \tag{90}$$

where k_n^i is the local channel wavenumber in sector i. Note specifically that we are expanding about the right-hand-side of each sector, because it simplifies the propagation of the overlaps. Next we define primitive overlap integrals of the bound function(s) in sector i,

$$[\underline{N}_s^i]_{nm} = \int_{R_i^-}^{R_i^+} \mathcal{F}_n(R,r)\; s_m(R;i)\; F_m(r;i)\; dR, \tag{91}$$

$$[\underline{N}_c^i]_{nm} = \int_{R_i^-}^{R_i^+} \mathcal{F}_n(R,r)\; c_m(R;i)\; F_m(r;i)\; dR. \tag{92}$$

Note that if $\mathcal{F}_n(R,r) = \delta(R-R_o^n)\;\delta(r-r_o^n)$, or is a narrow gaussian[109,110] centered at (R_o^n, r_o^n), then the integrals above are easily evaluated.

If $\underline{R}(i)$ is the global R matrix accumulated after propagating through sector i, we then compute from it a local overlap in sector i,

$$\underline{d}(i) = \underline{N}_s^i \cdot [\underline{R}(i)\cdot \underline{k}^i]^{-1} + \underline{N}_c^i, \tag{93}$$

and a matrix relating overlaps in sector i to those in sector i+1,

$$\underline{Q}(i,i+1) = \underline{T}(i,i+1)\cdot \left[\underline{s}(R_-^{i+1})\cdot [\underline{R}(i+1)\cdot \underline{k}^{i+1}]^{-1} + \underline{c}(R_-^{i+1})\right], \tag{94}$$

where $\underline{T}$ is defined in Eq. (45), and the diagonal $\underline{s}$ and $\underline{c}$ matrices are defined in Eq. (90). The accumulated overlap through sector i+1 is now given by

$$\underline{D}(i+1) = \underline{d}(i+1) + \underline{D}(i)\cdot \underline{Q}(i,i+1). \tag{95}$$

The overlap propagation begins with $\underline{D}(1) = \underline{d}(1)$ and continues through the sector where boundary conditions are imposed. At this point we compute the desired overlap matrix by taking the same linear combination of the propagated overlaps as for asymptotic boundary conditions (see Eq. (74)),

$$\underline{\mathcal{K}} = \underline{D}(\text{final})\cdot \left[\underline{\mathcal{J}} - \underline{\mathcal{O}}\cdot \underline{k}^{-1/2}\cdot \underline{S}^J \cdot \underline{k}^{1/2}\right]. \tag{96}$$

It should also be clear that a similar approach could be employed, if desired, to propagate overlaps of bound state wavefunctions with the gradient of the scattering wavefunction. Note from Eqs. (93)-(94) that the propagation of overlaps requires at each step an inversion of the R matrix; if one propagates the log-derivative matrix[76] instead of the R matrix, then the propagation of overlaps by this scheme requires only a few additional matrix multiplications at each step.

5. SUMMARY

The Bending Corrected Rotating Linear Model should be useful as a tool for insight into the importance of some of the three-dimensional features expected of collinearly dominated atom-diatom reactions. The Rotating Linear Model, defined by Child,[1] Connor and Child,[3] and by Wyatt,[2] augments the collinear world naturally with an impact parameter, making it possible to compute integral and differential cross sections. Adding a bending correction then improves the quantitative predictive ability of the method, and permits a more direct comparison with 3D rotationally averaged integral cross sections and rate constants.

Additional theoretical refinement is needed before we can quantitatively compare BCRLM differential cross sections with 3D. The shape of the BCRLM differential cross section contains information about the impact parameter dependence of the reaction probability, and whenever the 3D angular distribution retains only this level of dynamical detail, we would expect the BCRLM differential cross section to compare nicely. Consequently, it is likely that BCRLM will fare best when compared to 3D differential cross sections from the ground state of reactants to all product rotational states, since this type of cross section retains the least amount of rotational information.

REFERENCES

1. M. S. Child, Mol. Phys. 12, 401 (1967).
2. R. E. Wyatt, J. Chem. Phys. 51, 3489 (1969).
3. J. N. L. Connor and M. S. Child, Mol. Phys. 18, 653 (1970)
4. D. W. Jepsen and J. O. Hirschfelder, J. Chem. Phys. 30, 1032 (1959)
5. N. Agmon, Chem. Phys. 61, 189 (1981)
6. G. C. Schatz and A. Kuppermann, J. Chem. Phys. 62, 2502 (1975)
7. A. B. Elkowitz and R. E. Wyatt, J. Chem. Phys. 62, 2504 (1972)
8. A. B. Elkowitz and R. E. Wyatt, J. Chem. Phys. 63, 702 (1975)
9. R. E. Wyatt, ACS Symp. Ser. No. 56, edited by P. R. Brooks and E. F. Hayes (American Chemical Society, Washington, D. C., 1977), p. 185.
10. G. C. Schatz and A. Kuppermann, J. Chem. Phys. 65, 4642 (1976)
11. G. C. Schatz and A. Kuppermann, J. Chem. Phys. 65, 4668 (1976)
12. R. E. Wyatt, in *Atom-Molecule Collision Theory*, edited by R. B. Bernstein, (Plenum, New York, 1979), p. 567.
13. R. B. Walker, E. B. Stechel, and J. C. Light, J. Chem. Phys. 69, 2922 (1978)
14. R. B. Walker, J. C. Light, and A. Altenberger-Siczek, J. Chem. Phys. 64, 1166 (1976)
15. R. B. Walker and E. F. Hayes, J. Phys. Chem. 87, 1255 (1983)
16. E. M. Mortensen and K. S. Pitzer, Chem. Soc. (London), Spec. Publ. 16, 57 (1962)
17. E. M. Mortensen, J. Chem. Phys. 48, 4029 (1968)
18. J. M. Bowman, G. Z. Ju, and K. T. Lee, J. Chem. Phys. 75, 5199 (1981)

19. J. M. Bowman, G. Z. Ju, and K. T. Lee, J. Phys. Chem. 86, 2232 (1982)
20. J. M. Bowman, K. T. Lee, and G. Z. Ju, Chem. Phys. Lett. 86, 384 (1982)
21. K. T. Lee and J. M. Bowman, J. Phys. Chem. 86, 2289 (1982)
22. J. M. Bowman and K. T. Lee, Chem. Phys. Lett. 94, 363 (1983)
23. J. M. Bowman, K. T. Lee, and R. B. Walker, J. Chem. Phys. 79, 3742 (1983)
24. J. M. Bowman, Adv. Chem. Phys. (to be published)
25. B. C. Garrett and D. G. Truhlar, J. Am. Chem. Soc. 101, 4534 (1979)
26. B. C. Garrett and D. G. Truhlar, J. Phys. Chem. 83, 1915 (1979)
27. B. C. Garrett and D. G. Truhlar, Proc. Natl. Acad. Sci. USA 76, 4755 (1979)
28. B. C. Garrett and D. G. Truhlar, J. Chem. Phys. 72, 3460 (1980)
29. B. C. Garrett, D. G. Truhlar, R. S. Grev, and A. W. Magnuson, J. Phys. Chem. 84, 1730 (1980)
30. B. C. Garrett, D. G. Truhlar, and R. S. Grev, J. Phys. Chem. 84, 1749 (1980)
31. D. G. Truhlar, A. D. Isaacson, R. T. Skodje, and B. C. Garrett, J. Phys. Chem. 86, 2252 (1982)
32. B. C. Garrett and D. G. Truhlar, "Generalized Transition State Theory and Least-Action Tunneling Calculations for the Reaction Rates of H(D) + H_2(n=1) → H_2(HD) + H," to be published, J. Phys. Chem.
33. T. Carrington and W. H. Miller, J. Chem. Phys. 81, 3942 (1084)
34. R. A. Marcus, J. Chem. Phys. 45, 4493 (1966)
35. R. A. Marcus, J. Chem. Phys. 49, 2610 (1968)
36. R. E. Wyatt, J. Chem. Phys. 56, 390 (1972)
37. C. C. Rankin and J. C. Light, J. Chem. Phys. 51, 1701 (1969)
38. G. Miller and J. C. Light, J. Chem. Phys. 54, 1635 (1971)
39. L. M. Delves, Nucl. Phys. 9, 391 (1959); 20, 275 (1960)
40. A. Kuppermann, Chem. Phys. Lett. 32, 374 (1975)
41. G. Hauke, J. Manz, and J. Romelt, J. Chem. Phys. 73, 5040 (1980)
42. A. Kuppermann, J. A. Kaye, and J. P. Dwyer, Chem. Phys. Lett. 74, 257 (1980)
43. J. Romelt, Chem. Phys. Lett. 74, 263 (1980)
44. B. R. Johnson, J. Chem. Phys. 73, 5051 (1980)
45. D. K. Bondi and J. N. L. Connor, Chem. Phys. Lett. 92, 570 (1982)
46. V. Aquilanti, G. Grossi, and A. Lagana, Chem. Phys. Lett. 93, 174 (1982)
47. J. M. Launay and M. Le Dourneuf, J. Phys. B15, L455 (1982)
48. D. K. Bondi, Ph.D. Thesis, University of Manchester, 1985, preprint kindly provided by J. N. L. Connor.
49. J. C. Light and R. B. Walker, J. Chem. Phys. 65, 4272 (1976)
50. J. Manz and J. Romelt, Chem. Phys. Lett. 76, 337 (1980)
51. J. Manz and J. Romelt, Chem. Phys. Lett. 77, 172 (1981)
52. J. Manz and J. Romelt, Chem. Phys. Lett. 81, 179 (1981)
53. J. Manz, E. Pollak, and J. Romelt, Chem. Phys. Lett. 86, 26 (1982)
54. J. Romelt, Chem. Phys. Lett. 87, 26 (1982)

56. J. A. Kaye and A. Kuppermann, Chem. Phys. Lett. 77, 573 (1981)
57. J. A. Kaye and A. Kuppermann, Chem. Phys. Lett. 78, 546 (1981)
58. V. Aquilanti, S. Cavalli, and A. Lagana, Chem. Phys. Lett. 93, 179 (1982)
59. V. Aquilanti, Hyperfine Interactions 17-19, 739 (1984)
60. V. Aquilanti, S. Cavalli, G. Grossi, and A. Lagana, J. Molec. Structure 93, 319 (1983)
61. V. Aquilanti, S. Cavalli, G. Grossi, and A. Lagana, J. Molec. Structure 107, 95 (1984)
62. B. Podolsky, Phys. Rev. 32, 812 (1928)
63. H. Margenau and G. M. Murphy, *The Mathematics of Physics and Chemistry*, 2nd Edition (D. Van Nostrand, Inc., Princeton, 1956), pp. 192-7.
64. R. B. Walker and E. Pollak, J. Chem. Phys. 83, 0000 (1985)
65. R. B. Walker and E. F. Hayes, J. Phys. Chem. 88, 1194 (1984)
66. E. F. Hayes and R. B. Walker, J. Phys. Chem. 88, 3318 (1984)
67. E. F. Hayes and R. B. Walker, ACS Symp. Ser. No. 263, edited by D. G. Truhlar (American Chemical Society, Washington, D. C., 1984), p. 493
68. R. B. Walker, N. C. Blais, and D. G. Truhlar, J. Chem. Phys. 80, 246 (1984)
69. R. Steckler, D. G. Truhlar, B. C. Garrett, N. C. Blais, and R. B. Walker, J. Chem. Phys. 81, 5700 (1984)
70. A. Lagana, contribution in this volume.
71. B. M. D. D. Jansen op de Haar, G. G. Balint-Kurti, and R. E. Wyatt, "An Approximate Three-Dimensional Quantum Mechanical Calculation of Reactive Scattering Cross Sections for the H + $Cl_2(v) \rightarrow HCl(v') +$ Cl Reaction," preprint.
72. W. H. Miller, private communication.
73. R. B. Walker, QCPE Program No. 352, Department of Chemistry, Indiana University, Bloomington, IN
74. E. B. Stechel, R. B. Walker, and J. C. Light, J. Chem. Phys. 69, 3518 (1978)
75. J. C. Light, R. B. Walker, E. B. Stechel, and T. G. Schmalz, Computer Phys. Comm. 17, 89 (1979)
76. J. C. Light, contribution in this volume.
77. D. J. Zvijac and J. C. Light, Chem. Phys. 12, 237 (1976)
78. R. D. Levine and R. B. Bernstein, *Molecular Reaction Dynamics*, (Oxford University Press, New York, 1974), p. 108.
79. E. Pollak and R. E. Wyatt J. Chem. Phys. 78, 4464 (1983)
80. R. A. Marcus, J. Chem. Phys. 45, 2138 (1966); K. Morokuma, B. C. Eu, and M. Karplus, J. Chem. Phys. 51, 5193 (1969)
81. N. Abu-Salbi, D. J. Kouri, Y. Shima, and M. Baer, J. Chem. Phys. 82, 2650 (1985)
82. N. Abu-Salbi, D. J. Kouri, Y. Shima, and M. Baer, Chem. Phys. Lett. 105, 472 (1984)
83. E. B. Gordon, B. I. Ivanov, A. P. Perminov, V. E. Balalaev, A. N. Ponomarev, and V. V. Filatov, Chem. Phys. Lett. 58, 425 (1978)

85. H. R. Mayne and J. P. Toennies, J. Chem. Phys. 75, 1794 (1981)
86. P. Siegbahn and B. Liu, J. Chem. Phys. 68, 2457 (1978); B. Liu, *ibid*. 58, 1925 (1973)
87. D. G. Truhlar and C. J. Horowitz, J. Chem. Phys. 68, 2466 (1978); 71, 1514 (E) (1979)
88. M. J. Redmon and R. E. Wyatt, Chem. Phys. Lett. 63, 209 (1979)
89. R. E. Wyatt, in *Horizons in Quantum Chemistry*, edited by K. Fukui and B. Pullman, (Reidel, Dordrecht, 1980), p. 63.
90. R. E. Wyatt, J. F. McNutt, and M. J. Redmon, Ber. Bunsenges. Phys. Chem. 86, 437 (1982)
91. R. E. Wyatt and M. J. Redmon, Chem. Phys. Lett. 96, 284 (1983)
92. M. Baer, J. Jellinek, and D. J. Kouri, J. Chem. Phys. 78, 2962 (1983)
93. S. H. Suck, Chem. Phys. Lett. 77, 390 (1981)
94. S. H. Suck and R. W. Emmons, Phys. Rev. A 24, 129 (1981)
95. R. W. Emmons and S. H. Suck, Phys. Rev. A 25, 178 (1982)
96. D. G. Truhlar, B. C. Garrett, and N. C. Blais, J. Chem. Phys. 80, 232 (1984)
97. N. Abusalbi, D. J. Kouri, Y. Shima, and M. Baer, Chem. Phys. Lett. 105, 472 (1984)
98. G. C. Schatz, J. Chem. Phys. 79, 5386 (1983)
99. E. Pollak and R. E. Wyatt, Chem. Phys. Lett. 110, 340 (1984)
100. E. Pollak, J. Chem. Phys. 83, 1111 (1985)
101. G. G. Balint-Kurti, private communication.
102. E. Pollak, N. Abusalbi, and D. J. Kouri, Chem. Phys. Lett. 113, 585 (1985)
103. N. Abu-Salbi, D. J. Kouri, M. Baer, and E. Pollak, J. Chem. Phys. 82, 4501 (1985)
104. Y. B. Band, K. F. Freed, and D. J. Kouri, J. Chem. Phys. 74, 4380 (1980)
105. G. G. Balint-Kurti and M. Shapiro, Chem. Phys. 61, 137 (1981)
106. K. C. Kulander and J. C. Light, J. Chem. Phys. 73, 4337 (1980)
107. M. Shapiro and R. Bersohn, Ann. Rev. Phys. Chem. 33, 409 (1982)
108. B. I. Schneider and H. S. Taylor, J. Chem. Phys. 77, 379 (1982)
109. J. C. Light, I. P. Hamilton, and J. V. Lill, J. Chem. Phys. 82, 1400 (1985)
110. I. P. Hamilton and J. C. Light, "On Distributed Gaussian Bases for Multi-dimensional Vibrational Problems," preprint.